Characterizing mass, charge, and radius of Lycopodium spores using electrical trapping and optical imaging techniques

Mähring, Marcus[1]

[1]ETH Zürich
30.12.2021

Abstract

This article aims to measure the typical mass, charge, and radius of charged lycopodium spores using a Paul trap (quadrupole trap) and elementary experimental techniques. These included but were not limited to powder diffraction measurements, high-resolution imaging, and terminal velocity measurements in a laminar flow. The experiment was facilitated by laser sampling in an ion trap controlled using Raspberry Pi GPIO utilities. The terminal velocity assumption of the particle experiencing laminar flow was also verified, as the Reynolds numbers for the different scenarios all were < 1. The experiment found that of a sample size of 15 particles, they had an average mass of $\bar{m} = (59.5 \pm 4.7)\,\mathrm{ng}$. The average radius varied, depending on the experimental method, between $(10.51 \pm 0.57)\,\mu\mathrm{m}$, and $(17.8 \pm 1.7)\,\mu\mathrm{m}$, from which the typical charge was determined to be about $(249 \pm 49) \times 10^3$ unit charges. Finally, the author discusses the underlying distribution of the variables based upon the available data and finds it requires a more thorough investigation and a larger sample size to rectify the assumptions of an underlying normal distribution.

Contents

1 Introduction

In this experiment, we use a quadrupole trap, a trap made to confine charged particles in space using electric fields. Ion trapping and investigating has been a staple of research in the physical sciences since its introduction and is still facilitating new experimental techniques, and studies [1][2]. In this experiment, a Paul trap, laser diffraction, and fall in laminar flow are employed to investigate lycopodium spores: namely their average radius, mass, and the charge they carry.

1.1 Theory of the trapping configuration

In creating the trapping configuration, we must first recall that the electric fields must be dynamic from Maxwell's equations (Gauss' law). I.e., no electrostatic field can satisfy the electric field we require. Therefore, the solution used is combining an electrostatic field and an oscillating field at a determined frequency Ω [1].

In the case where the particle performs a motion which is slow relative to the trapping potential, the average effect of the switching field will be such that it traps the particle at a potential minimum. Thus we can write the total potential as [1]:

$$\Phi(\mathbf{r}, t) = \Phi_{\mathrm{DC}}(\mathbf{r}) - \Phi_{\mathrm{AC}}(\mathbf{r}) \cos \Omega t$$

with Φ_{DC} and Φ_{AC} the static and oscillating components of the potential respectively. Now, in a 2D plane, we consider the dynamic part and expand it around $\vec{r} = 0$, which leads one to a modulated harmonic potential. The movement of the ion in this potential is separable. For a more thorough derivation, see [1]. The above consideration gives the *Mathieu differential equation*:

$$\frac{\partial^2 x}{\partial t^2} = -\frac{q}{m}\frac{\partial \Phi}{\partial x} = \frac{q}{m}(Cx \cos \Omega t)$$

with C a constant determined in the above argumentation. Defining $\tau = \frac{\Omega t}{2}$ and $q_x = \frac{2qCx}{m\Omega^2}$ and solving the resulting differential equation in the limit $q_x \ll 1$, one gets:

$$x(t) = C_i \cos(\beta\tau) \left[1 - \frac{q_x}{2} \cos(2\tau)\right]$$

with $\beta = |q_x|/\sqrt{2}$. Noting $|q_x| \ll 1$ the motion of the particles will be dominated by the slower oscillation of $\omega_s = \beta\Omega/2 \ll \Omega$, in turn regulated by a smaller oscillation with a higher frequency Ω, the oscillation frequency of the AC voltage. The former is the *secular motion* of the particle and the latter the *micromotion* [1].

The secular motion represents the average effect of the fast oscillating electric field. Thus

greater displacements around equilibrium due to outside forces lead to greater restoring forces from the pseudopotential, which induces the secular motion.

1.2 The electric field in the center of the trap

In this part, a few sample problems are solved to extrapolate some general properties of our trapping configuration. In general, we wish to solve the Poisson equation for the electric potential and then take the negative gradient to find the electric field. For these problems, the Dirichlet boundary conditions (we know the potential on the boundary) will be used to impose uniqueness of the solution [3].

1.2.1 Two parallel plates

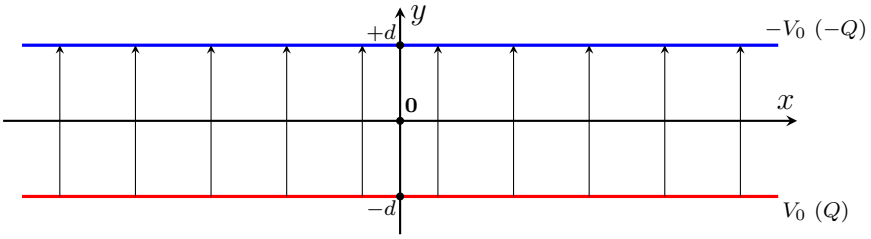

Figure 1: In the figure, the configuration of two parallel plates with a negative potential on the upper plate and positive potential of equal magnitude on the lower plate. These plates are assumed to be infinitely long. One should note the symmetry of the configuration: if one should switch the polarity of the two plates, the vector $\hat{r}$ in equation (1) switches sign.

We have the configuration as displayed in figure 1. Here we note that the derivative of our potential is constant, leading us to calculate the derivative of the potential – the magnitude of the electric field – by finding the potential difference of the two plates. In addition, we note that a positive particle in the above configuration will move towards the upper (negatively charged) plate to find the direction. In other terms:

$$\vec{E} = \frac{\Delta V}{\Delta r}\hat{r} = \frac{V_0 - (-V_0)}{2d}\hat{r} = \frac{V_0}{d}\hat{r} \qquad \hat{r} = \begin{pmatrix} 0 \\ 1 \end{pmatrix} \tag{1}$$

1.2.2 One electrode

Recall the general form of potential in cylindrical coordinates with cylindrical symmetry (symmetry in the z coordinate) [3]:

$$V(r,\phi) = a_0 \ln(r) + b_0 + \sum_{m=1}^{\infty} \left[\left(A_m r^m + \frac{B_m}{r^m} \right) \cdot (C_m \cos(m\phi) + D_m \sin(m\phi)) \right]$$

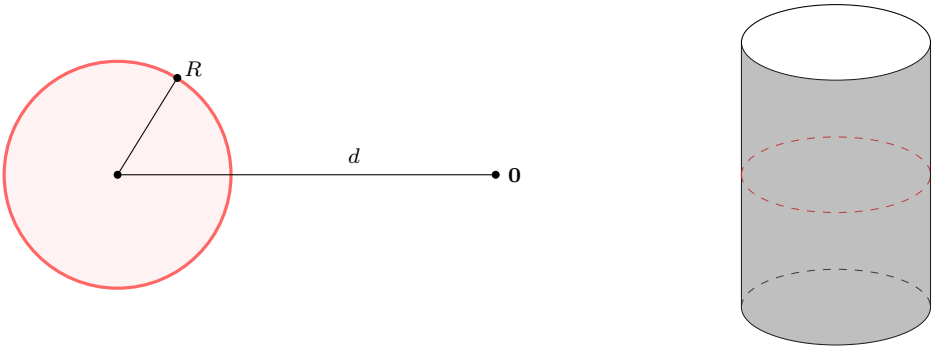

Figure 2: The setup for the one electrode problem. We have a cylindrical symmetry and solve for the potential this electrode with constant surface potential produces in the plane. Additionally, we impose the potential shall obey $V(0) = 0$: it must vanish in the origin.

We now note that at the boundary of our cylinder the solution should match the surface potential, which has no angular part, i.e. $C_m = D_m = 0 \; \forall m$. Thus, at the boundary:

$$V_0 \stackrel{!}{=} a_0 \log(R) + b_0$$

With R being the radius of the cylinder. Additionally imposing $V(d) \stackrel{!}{=} 0$ (d being the distance to the center of the trap) we get the additional equation:

$$0 \stackrel{!}{=} a_0 \log(d) + b_0$$

Thus implying:

$$a_0 = \frac{V_0}{\log(R/d)} \qquad b_0 = -\frac{V_0 \cdot \log(d)}{\log(R/d)}$$

Which gives the solution for the potential:

$$V(r, \phi) = \frac{V_0}{\log(R/d)} \big(\log(r) - \log(d) \big)$$

and the solution for the electric field ($\vec{E} = -\vec{\nabla} V$):

$$\vec{E}(r) = \frac{V_0}{\log(d/R)} \cdot \frac{\hat{r}}{r} \tag{2}$$

1.2.3 The general case and calculating q/m values

Combining the above results, (1) and (2), we expect the general E-field in the middle of the trap to be of the following form:

$$E_{\text{Mid}} = \alpha \frac{V_0}{d} \tag{3}$$

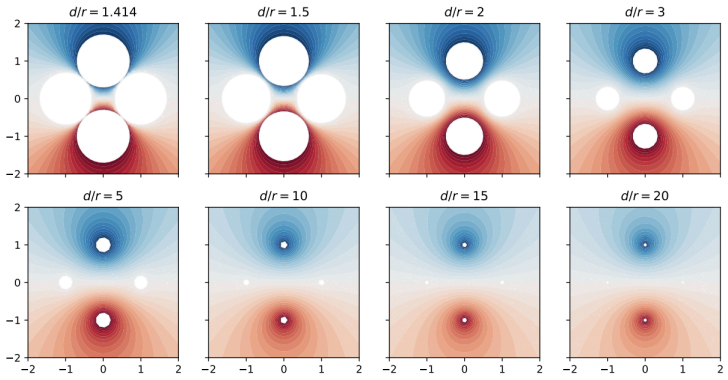

Figure 3: Some simulated electric fields for different trap geometries. [1]

Where α is some scaling constant for the trap geometry. However, the trap geometry in the case of four electrodes with constant surface potential is not analytically solvable [1][3]. Thus one must rely on for instance the finite element method (FEM). In figure 3 some sample simulated traps with different distances radii of the electrodes in combination with different distances from the center of an electrode to the center of the trap represented by the d/r ratio. In section 3 some α for different d/r rations are given together with the first order approximation of the correction factor as in equation (2) (figure 16) [1].

If the DC voltage is applied in such a way that the micromotion is minimized, i.e. the electric force is in equilibrium with the gravitational force we get the following relation:

$$mg = qE_c \quad \Longrightarrow \quad \frac{q}{m} = \frac{g}{E_c} \tag{4}$$

Where m is the mass, g is the gravitational acceleration, q is the charge, and finally, E_c is the bias electric field in the trap's center.s If we know the bias electric field in the center of the trap, the mass, and the distribution of charge per mass coupled with the average mass, we can approximate the charge of the individual (clusters of) particles.

$$q_{\text{Particle}} = \bar{m}\frac{g}{E_c} \tag{5}$$

1.3 Determining radius through diffraction

Let R denote the average radius of the particles we wish to measure, R_A is the radius to the first minimum of the airy disc. We define D as the distance between the sample and the screen for convenience. Finally, H denotes the hypotenuse in the right-hand triangle formed by R_A and D.

By analyzing the zeros of the first-order Bessel function we can find an expression linking the position of the first minimum to the geometry of the setup, and the quantities λ and

R [1] [4]:

$$\sin\theta \simeq 1.22\frac{\lambda}{2R} \tag{6}$$

where, 1.22 approximately is the first zero of the first-order Bessel function $J_1(x)$ divided by π. Due to 1.22 being an excellent approximation of this number[1] no distinction shall be made in following. R is the average radius of the particles in the sample and λ the wavelength of the laser.

To find an expression of the radius of the spores, we employ a common approximation used in conjunction with Fraunhofer diffraction: a small-angle approximation. Here we assume $\theta \approx 0$, which is exactly the case is D is big in relation to R_A, defined in figure 4:

$$\sin\theta \approx \tan\theta = \frac{R_A}{D}$$

Thus the equation to solve for R becomes:

$$R \simeq \frac{1.22\lambda D}{2R_A} \tag{7}$$

1.4 Terminal velocity

For a particle falling in laminar flow[2] (relatively slowly, keeping the turbulent forces low) the drag of the particle is given by Stokes' law [5]:

$$F_d = -6\pi\mu R v \stackrel{!}{=} -mg \tag{8}$$

where $\mu = 1.8 \times 10^{-5}\,\mathrm{kg/(m\,s)}$ is the dynamic viscosity of air, R is the radius of the falling particle and is v the velocity. When v is the terminal velocity, the right side of the equation holds [4]. This is equivalent to the following relation at terminal velocity v_T for the mass, m:

$$\frac{m}{R} = \frac{6\pi\mu}{g} v_T \tag{9}$$

[1] $||1.22 - x_0/\pi|| \sim 10^{-4}$, with x_0 the first zero of $J_1(x)$.

[2] Note that this only holds for particles with radii $< 1\,\mu\mathrm{m}$. If the radius is lower than this value, the non-continuum of the gas medium becomes apparent, and correction terms are needed [5].

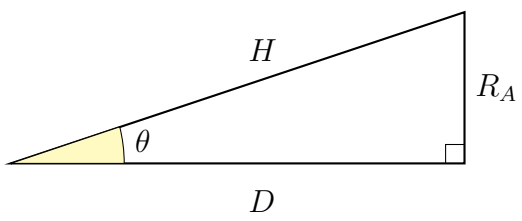

Figure 4: The geometrical setup of the diffraction experiment.

Additionally, the validity of the above result may be investigated if one can certify that the flow around the falling particle is laminar. The quotient of viscous to turbulent forces is quantified by calculating the Reynolds number for the scenario [1]. If $Re \ll 1$ for the situation, the approximation that there is no turbulent flow is valid, and thus we can apply equation (8) [5].

$$Re = \frac{2\rho v_T R}{\mu} \tag{10}$$

Here $\rho = 1.2\,\mathrm{kg/m^3}$ is the density of air at atmospheric pressure and v_T the terminal velocity [1] [5].

The mass and size (radius) of were estimated to be $m = 2.5\,\mu\mathrm{g}$ and $r = (25 \pm 10)\,\mu\mathrm{m}$. The mass was estimated by taking something of the same order of magnitude as the radius, which was easier to estimate. The radius estimate was found by comparing the spores to the thickness of a strand of hair. If the estimate of the radius is found to be true, and v_T be of the order, $\sim 300\,\mathrm{mm/s}$ and the Reynolds number should satisfy the condition $Re \sim 0.1 \ll 1$, thus implying a laminar flow, in which case Stokes law is valid [5].

2 Method

The experimental method was divided into distinct parts, each aiming to determine a characteristic of the lycopodium particles to facilitate the ultimate determination of the charge. First, an outline of the experimental methods is given, then the results are presented, followed by a discussion thereof.

2.1 Setup, calibration and initial observations

2.1.1 Setup and calibration

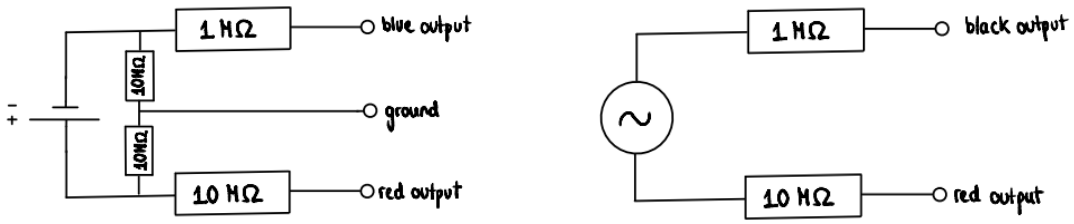

(a) The DC part of the safety box

(b) The AC part safety box

Figure 5: The wiring within the safety box [1]

A variac and a DC power supply were mounted to a safety box for the experiment. Firstly, the electrodes lying in the horizontal plane of the trap were then wired to the AC output of the safety box, effectively wiring them to the variac. Secondly, the bias electrodes in the vertical plane were wired to the DC output of the safety box with the upper being connected such as to carry negative current and the lower plates carrying positive current. Later in the experiment, this allows compensation of gravity by applying a bias electric field in the trap. Finally, the end-caps were all attached to the positive current, enabling a positively charged particle to be trapped.

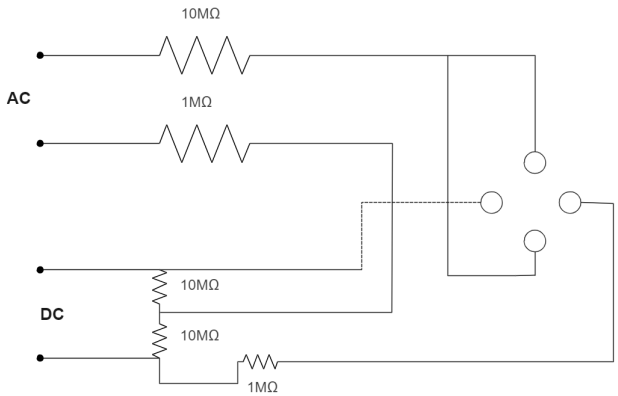

Figure 6: The wiring configuration of the bias section of the rods. Note that the high resistance resistors visible in the schematic belong to the safety box, in effect limiting the maximum current which could flow through an experimenters body. [1]

One should note that this configuration traps a *positively* charged particle, but in the case that one needs to trap a negative particle, the end-caps and the bias' (center segments) voltages signs should be switched. The effect of these modifications is that we create a trapping configuration for the particle in the middle of the trap and again allow compensation for gravity by applying a positive voltage.

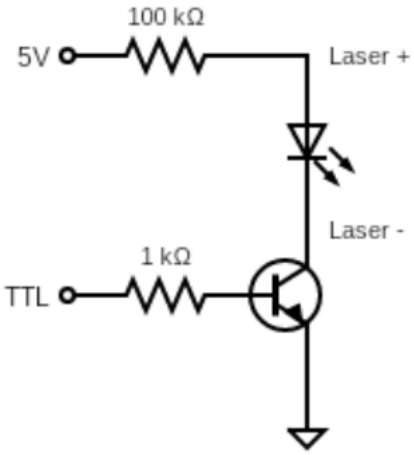

Figure 7: The driver circuit for the laser

Following the setup of the trap, the laser was connected to the driving circuit (see figure 7). The circuit consists of a 5 V connection from a Raspberry Pi GPIO header to a resistor of 100 kΩ and a transistor. The other end of the transistor was attached to a 3.3 V GPIO output pin (GPIO pin 13) which offers digital output as well as pulse-width modulation (PWM), allowing us to trigger the laser via the Raspberry Pi, effectively using the transistor as a switch.

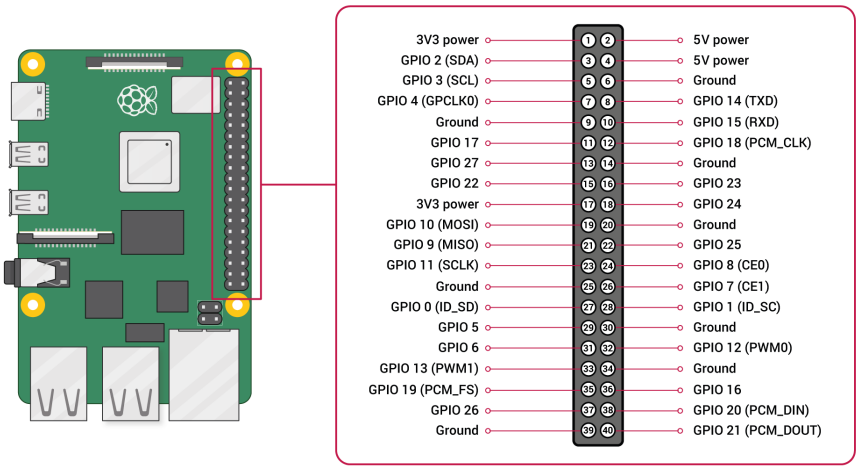

Figure 8: The general layout of the GPIO on the Raspberry Pi model 3b+. Note the pulse-width modulation (PWM) support on GPIO 13. [6]

The additional resistors described above serve the purpose of restricting the effective potential over the laser to allowed levels – $\leq 3.3\,\mathrm{V}$ – as well as regulating the current to the acceptable range of $\leq 25\,\mathrm{mA}$ (see appendix C for the datasheet of the laser) [1]. Finally, one should note that the Raspberry Pi GPIO header provides a maximum of 16 mA per pin, with a total of 50 mA being able to be provided over the entire header at any given moment [6].

After that, the laser was mounted on the trap. Then it was calibrated by adjusting its position, maximizing the amount of light let through holes in the trap mount. Thus, the beam-axis of the laser was aligned with the trap center.

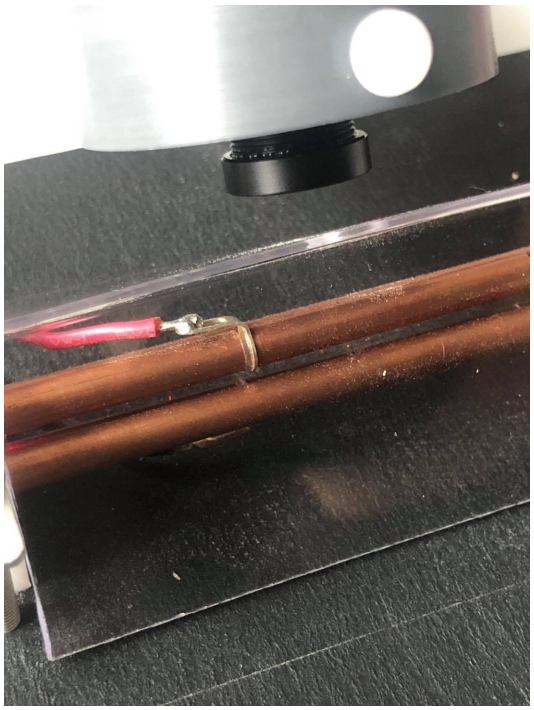

Figure 9: The camera mounted to look between the bias electrodes to observe the particles in the middle. The part of the upper electrode where the wire is mounted distinguishes between the bias and endcap parts of the electrode.

Next, a see-through plastic windshield was placed over the setup to assure that trapped particles were not pushed out of the trapping configuration due to external factors such as ventilation or movement in the laboratory. The shield also acts as additional protection for the operator by covering otherwise exposed wiring and current-carrying electrodes. Finally, a Raspberry Pi camera was focused on the trap center where the particles would be trapped.

2.1.2 Loading the trap and initial observations

Before loading the trap, the electricity was shut off, and the variac was set to 0% of its maximal voltage and then plugged in. Then the AC voltage was set to $(220 \pm 5)\,\mathrm{V}$

(oscillating at a frequency of 50 Hz) and the DC voltage to $(30.0 \pm 0.5)\,\mathrm{V}$[3], a small Teflon stick was rubbed against a piece of cloth to induce electrostatic charge. This stick was then dipped in a small pooling of lycopodium powder, making the powder stick to it by electrostatic attraction. It was then inserted into the trap through an opening in the windshield. It was subsequently shaken to get some powder trapped in the field.

Two different methods to observe the particles were investigated. Firstly the laser was kept on continuously while observing the particles, and afterward, the laser was flashed at a frequency of 49 Hz, 50 Hz and 51 Hz for 1 ms, effectively implemented by using a run-time $T = 20\,\mathrm{ms}$ at a 5% duty cycle.

2.2 Minimizing micromotion

To measure the mass/charge distribution, one can note that as mentioned in section 1 a particle outside of the natural zero of the pseudopotential will oscillate at a higher rate due to the greater restoring forces. Thus, by bringing the particle closer to the pseudopotentials center – effectively compensating for gravity – we can get determine q/m via equation (4).

The trap stability was first tested by observing a singular particle in the trap while slowly lowering the AC voltage – weakening the trapping stability – the DC voltage on the bias plates was then adjusted to minimize the micromotion of the particle. Notably, the maximum voltage which the DC source could deliver was around 32.5 V, imposing a restriction on which particles could be effectively minimized, as some particles may have needed a greater restoring potential, what this means in practice illuminating the particles with a continuous beam and then observing the trace of the motion of the particles in the field. This trace was observed through the pi-camera to obtain a more detailed view. Thereafter, the trace was minimized by adjusting the DC voltages.

The minimization of the micromotion was done by noting that the sensitivity to the particle's position on the z-axis increases when the AC voltage is lowered. Therefore, the procedure consisted of slowly reducing the AC voltage, and when a change in the particles' oscillation was detected, the DC voltage was adjusted accordingly to re-minimize this oscillation. The procedure was repeated until the particle escaped the trap due to the weak trapping (AC) voltage. Finally, the last DC value was noted.

[3]Note that these estimates are relatively unimportant, as the values of AC 220 and 30 are a starting point, indicating a reasonable range for the trapping configuration.

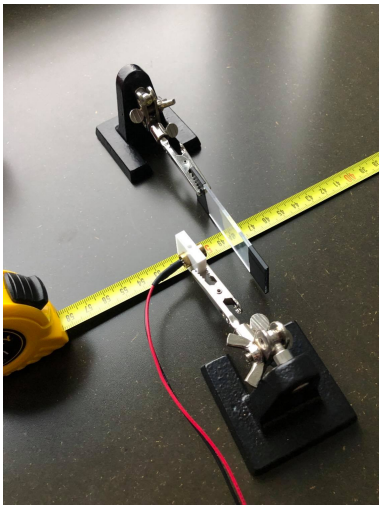

Figure 10: The laser mounted to illuminate the spores with the tape measure indicating the beam axis. Note how the sample and the laser are suspended of the table to project a more complete airy pattern on the screen.

2.3 Determination of the average lycopodium spore radius

In this section, the determination of the average radius is conducted in two separate attempts: once using diffraction at the scattered lycopodium powder and once taking a high-resolution photograph of the spores and a reference.

2.3.1 Determination through diffraction

Lycopodium was sandwiched between two glass plates and was then suspended in front of the laser mounted with a gripping claw aligning the beam axis of the laser. The axis was kept parallel to the table to avoid accidentally looking into the laser. The sample was held at a constant distant distance of $(50.0 \pm 0.4)\,\mathrm{cm}$ and the wavelength of the laser was read from the datasheet to be (655^{+5}_{-10}) nm (see appendix C for a complete data sheet), but with a typical output of 655 nm. The airy disc pattern was projected on a millimeter-marked disc affixed to the wall with some tape. The distance between two minima was then measured, from which the radius was calculated. From geometrical considerations, we can now determine the average radius of the lycopodium particles.

2.3.2 Determination by high-resolution photo

A photo of the sandwiched lycopodium spores suspended on a platform with a contrasting background was taken. The sample was then exchanged with an iPhone X, of which a photo was taken (see figure 11). Knowing the pixels per inch (PPI) value of the phone, 458, the distances in pixels can be converted to centimeters using:

$$L(P, P_r, \mathrm{PPI}) = P \cdot \frac{P_r}{458} \tag{11}$$

(a) A part of the photo of the phone screen of the iPhone X.

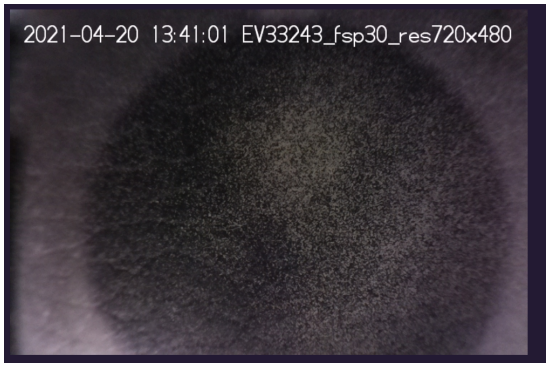

(b) A photo of the spores.

Figure 11: The first set of pictures used to determine the average spore size. If one sufficiently zooms in on the respective images, one can in 11a determine how many pixels equate to one inch and in 11b find objects which, with the resolution of the camera as the limiting factor, were determined to be (almost) individual particles, enabling one to measure the radii.

with P the length in pixels of the object (on the camera photograph), P_r the distance (in-camera image pixels) of one pixel on the iPhone screen, and finally, 458 being the PPI value of the iPhone X [7]. The reference length P_r was measured twice, and the mean was taken to get a better estimate, which was then used in converting the pixel radii into centimeters. The method was done twice.

2.4 Determination of the terminal velocity of lycopodium

2.4.1 Setup

A vertically aligned, transparent tube was illuminated from below with a laser to determine the lycopodium spores' terminal velocity. The tube was able to be reoriented as needed using adjustable screws. The positioning of the base place could also be adjusted by tuning the lengths of the screws. A detailed view of the setup is shown in figure 12.

2.4.2 Calibration

The calibration was done in two steps; in the first step, the laser was aligned with the tube, and in the second, the base plate was oriented such that the tube/beam axis was collinear to gravity.

A cap with a small hole was mounted on the tube to align the laser. Next, the laser was turned on, and the tube's orientation was adjusted with the screws until a bright red spot was visible on the ceiling. Afterward, the laser was turned off to change the cap.

Next, the tube was calibrated in the direction of gravity. This was done by installing a closed cap with a pendulum and turning on the laser. Then the table was realigned until

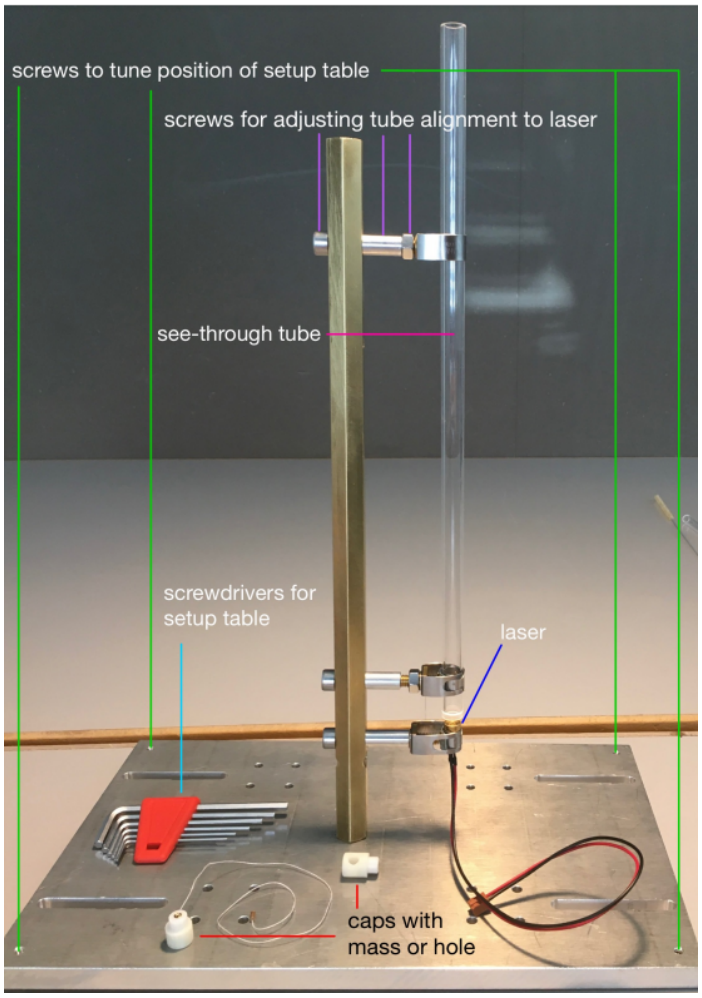

Figure 12: The setup for the terminal velocity experiment. Note how the laser is oriented toward the ceiling, allowing one to drop spores from the upper part of the tube and illuminate them with the laser. [1]

the string was continuously illuminated.

2.4.3 Measurements

The terminal velocity of the spores was measured by photographing them in free-fall. The distance traveled in one frame in pixels was used to calculate the speed through $v = \Delta s/\Delta t$. The principle measures the particle's terminal velocity falling in the air, which is assumed to be reached at the bottom. For reference to convert this value in [pixels/second], a pendulum of known dimensions was included in the shot, with diameter $(2.00 \pm 0.05)\,\mathrm{mm}$. In figure 13 the final setup is displayed with the camera.

The particles were then recorded while falling, and the laser was pulsed at different frequencies and different duty cycles. Additionally, the Pi-cameras ISO values and frame rate were adjusted to capture the falling spores better. The camera's exposure time was set to 500 ms and the framerate was then (depending on measurement series) varied between 10 and 30 FPS. The first measurement series was done at 10 FPS with a total

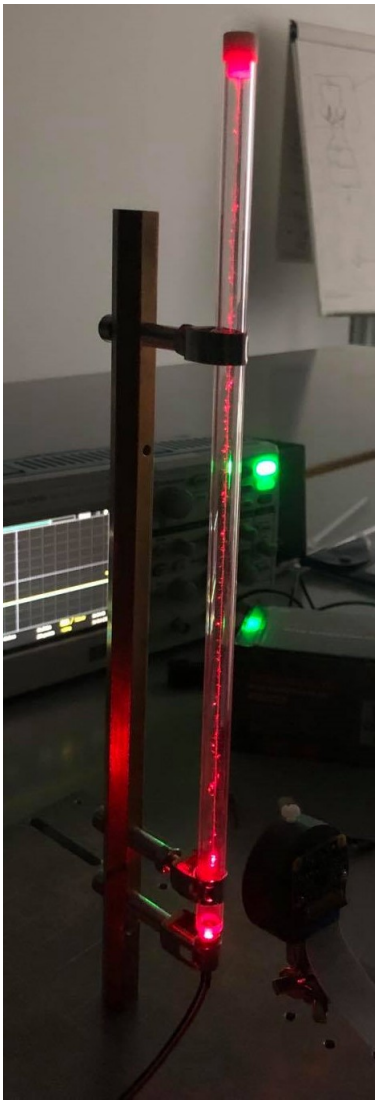

Figure 13: The setup during calibration of the camera with the continuous laser beam.

time-interval of 1 s with a duty cycle of 50% and a pulse frequency of 30 Hz. The second experiment was done at 20 FPS with 1 s with a duty cycle of 50% and at a frequency of 50 Hz.

By comparing the pictures taken by these two measurements, conclusions about the optimal settings for the experiment could be drawn.

3 Results and data analysis

3.1 Trap measurements

The trap dimensions were measured to be $2r = (3.00 \pm 0.25)$ mm (radius of the electrodes) and $d = (4.00 \pm 0.25)$ mm (d being the distance from the center of the trap to the middle of an electrode). This gives the proportion of the trap equal to: $d/r = 2.67 \pm 0.28$.

The error propagation can be derived as follows:

$$\sigma_{d/r} = \frac{1}{r}\sqrt{\frac{d^2}{r^2}\Delta r + \Delta d} \tag{12}$$

with $\sigma_{...}$ the standard deviation of the variable in the subscript and $\Delta...$ is the variance of the variable ($\sigma^2_{...} = \Delta...$).

3.2 Initial observations

The particle was successfully trapped, and one could observe several bright red spots in the middle of the trap illuminated by the laser— additionally, a fast oscillation in the transverse plane with occasional bigger displacement collinear to the beam axis. The particle was observed to be positively charged as it was trapped as described in section 2.

3.3 Sampling particle at 49, 50, 51 Hz (and continuously)

As mentioned, while using a continuous beam, traces from the particles were observed.

While flashing the laser, individual particles' were spontaneously illuminated, but no discernible difference could be observed between the different oscillation frequencies (49 Hz, 50 Hz, and 51 Hz). Why no difference was observed will be discussed later.

3.4 Stability of the trap

The stability of the trap for one particle was recorded for one individual particle to escape the trap at an AC value of 130 V and DC value of 30 V. The stability measurement was in practice repeated 15 more times in the next part, as the particles escaped the trap every time.

3.5 Minimizing micromotion

In table 1 the DC values as well minimizing micromotion for 15 different particles are given as well as the AC values before the particle leaves the trap. Later in the report the

scaling factor from equation (3) is determined to be $\alpha = 1.40 \pm 0.21$. We can determine the electric field in the middle of the trap for the different DC values by using this value together with equation (3). For the q/m values the error propagation of equation (4) is:

Measurement	AC [V]	DC [V]
1	150	14.5
2	80	31.5
3	90	30.5
4	70	27.2
5	120	16.1
6	50	20.3
7	90	25.4
8	85	25.3
9	75	26.8
10	130	29.1
11	125	22.7
12	90	19.9
13	60	29.3
14	105	23.6
15	85	27.5

Table 1: 15 measured values for some distinct separate particles. All DC values are recorded with the same degree of accuracy: about 0.05 V, and analogously the AC values with an accuracy of about 5 V

$$\sigma_{q/m} = \frac{1}{E_c}\sqrt{\frac{g^2}{E_c^2}\Delta E_c + \Delta g} \tag{13}$$

Using the above relations, we calculate the electric field in the center of the trap for the different DC values and derive the q/m values. These can be found in table 2.

Measurement	E-field [kV/m]	q/m [µC/g]
1	5.07 ± 0.82	1.93 ± 0.31
2	11.0 ± 1.80	0.89 ± 0.14
3	10.7 ± 1.70	0.92 ± 0.15
4	9.50 ± 1.50	1.03 ± 0.17
5	5.64 ± 0.92	1.74 ± 0.28
6	7.10 ± 1.20	1.38 ± 0.22
7	8.90 ± 1.40	1.1 ± 0.18
8	8.90 ± 1.40	1.11 ± 0.18
9	9.40 ± 1.50	1.05 ± 0.17
10	10.2 ± 1.70	0.96 ± 0.16
11	7.90 ± 1.30	1.23 ± 0.2
12	7.00 ± 1.10	1.41 ± 0.23
13	10.3 ± 1.70	0.96 ± 0.16
14	8.30 ± 1.30	1.19 ± 0.19
15	9.60 ± 1.60	1.02 ± 0.17

Table 2: The calculated electric field values and the q/m value to which they corresponds.

3.6 Measuring radius

3.6.1 Diffraction

The distance to the "screen" (measurement area) was as mentioned in section 2 measured to be (50.0 ± 0.4) cm and the typical wave-length was about (655 ± 5) nm. The distance *between two minima* on the screen were measured to $\delta = (3.8 \pm 0.2)$ cm, meaning the radius from the center of the airy disc to the first minima is $R_A = (1.9 \pm 0.1)$ cm.

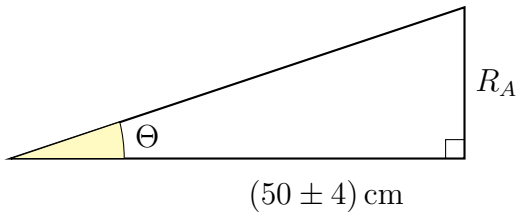

Figure 14: The geometrical setup of the diffraction experiment.

The measured value for the radius was calculated to be (10.51 ± 0.57) µm.

The error for the screen's distance was approximated from the fact that we could, in theory, measure to an estimated accuracy of 0.1cm, but in practice, we could only be precise within a margin of about double that distance. This uncertainty was doubled again as we could not precisely determine the position of the sample on the beamline. On the millimeter-marked screen, the uncertainty was estimated to consist of 0.1cm on each side of the airy pattern. The wavelength's uncertainty was estimated to be about 5nm, thus keeping it in range of the possible wavelengths on the datasheet about the typical output.

The error propagation using small-angle approximation is as follows:

$$\sigma_R \simeq \frac{1.22}{2R_A}\sqrt{\delta^2\Delta\lambda + \lambda^2\Delta\delta + \frac{\lambda^2\delta^2}{R_A^2}\Delta R_A} \tag{14}$$

3.6.2 High resolution image

The mean radius from the first image was (17.8 ± 1.7) µm and for the second image (17.6 ± 3.7) µm. The complete data can be seen in table 3.

For the error propagation, one should note that the uncertainty in PPI is zero (or at least close to zero in relation to the other errors in the experiment), leading to the removal of one term.

$$\sigma_L(P, P_r) = \frac{1}{\text{PPI}}\sqrt{\frac{PP_r}{\text{PPI}^2}\Delta\text{PPI} \ + P^2\Delta P_r + P_r^2\Delta P} \overset{\sigma_{PPI}=0}{=} \frac{1}{\text{PPI}}\sqrt{P^2\Delta P_r + P_r^2\Delta P} \tag{15}$$

Particle	Radius (set 1) [µm]	Radius (set 2) [µm]
1	24.7 ± 4.8	13.4 ± 4.0
2	24.7 ± 3.6	13.4 ± 3.0
3	21.0 ± 3.4	19.0 ± 4.8
4	16.5 ± 3.2	17.0 ± 5.6
5	21.0 ± 3.4	19.0 ± 4.8
6	16.5 ± 2.0	17.0 ± 4.5
7	13.0 ± 1.8	25.5 ± 7.8
8	10.5 ± 1.7	13.4 ± 4.0
9	13.0 ± 1.8	25.5 ± 7.8
10	16.5 ± 2.0	13.4 ± 5.2

Table 3: In this table, ten measured radii from the respective pictures are given in micrometers. The errors were determined individually for each particle. For some particles, it was clear where the particle ended. The error was then propagated together with the uncertainty for the length of one pixel on the iPhone. Here the resolution of the camera was the limiting factor. Note how some nominal values are the same but with different errors. The cause was that some clusters were better resolved than others.

3.7 Terminal velocity and the Reynolds number

From observing the taken pictures, one could confirm that the photos taken with a high pulsing frequency respective the frame rate (20 FPS with 1 s, 50% duty cycle and a frequency of 50 Hz) of the camera produced photos where one could observe distinct traces of the particle. Because the pulsing frequency was higher than the frame rate, one could also see several traces after one another. This allowed one to measure the spacing between the end of one trace and the start of another. Using this, one can confirm whether the particle had reached terminal velocity.

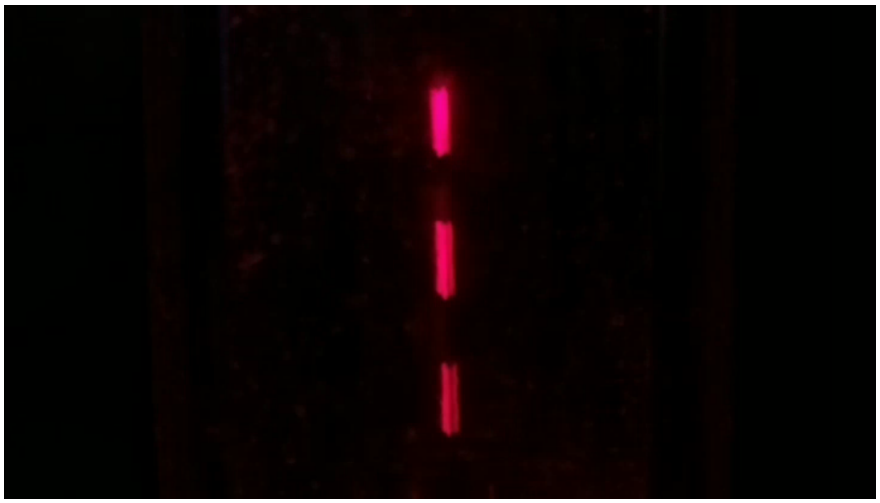

Figure 15: An example of a photo of particles falling in terminal velocity can be seen by noting the constant distance between the endpoints of one trace to the starting point of the next. We note that this is the same particle captured three times, which is logical, as we sample at 50 Hz and capture images at 20 FPS, we expect to find them on average about $\frac{50}{20} = 2.5$ times.

The terminal velocity was measured for 17 such particles and the mean was determined to be $(112.40 \pm 40.29)\,\mathrm{mm/s}$ ($\frac{\delta s}{\delta t}$). The error propagation for the terminal velocity follows:

$$\sigma_v = v\sqrt{\frac{1}{\delta s^2}\Delta v + \frac{1}{\delta t^2}\Delta s} \tag{16}$$

The value for the average mass-radius was determined by using the constants given in (8) using an error corresponding to half the last known digit and using the gravitational acceleration $g = (9.806\,000 \pm 0.000\,005)\,\mathrm{m/s^2}$. This value was retrieved from the website of the Federal Bureau for Meteorology (METAS) [8].

The calculated mass/radius value was then calculated to be $(38.9 \pm 1.2) \times 10^{-7}\,\mathrm{kg/m}$ using (9). The average mass was then determined by multiplying this quotient with the different measured radii and taking the average of these values. The average mass was thus determined to be about $(59.5 \pm 4.7)\,\mathrm{ng}$. The error propagation for the mass (see equation (8)) follows:

$$\sigma_m = \frac{6\pi\mu}{g}\sqrt{\frac{R^2 v_T^2}{g^2}\Delta g + v_T^2 \Delta R + R^2 \Delta v_T} \tag{17}$$

Regarding the Reynolds number, as noted in equation (10), it is a function of the radius as well as the velocity. Thus, we get different Reynolds numbers for the average velocity calculated above for our different measured radii. These are displayed in table 4.

	Diffraction	Phone 1	Phone 2
$Re\ [\cdot 10^{-2}]$	15.8 ± 1.2	26.6 ± 2.8	26.4 ± 5.7
Maximal possible $Re\ [\cdot 10^{-2}]$	16.9	29.5	32.1

Table 4: Reynolds numbers for the experiment with the diffraction and phone are given in terms of 10^{-2}. Additionally given is the upper bound of the previously mentioned Reynolds numbers, derived from the error of the variables. The values given are rounded to the nearest decimal.

The error propagation for the equation of the Reynolds number is:

$$\sigma_{Re}(v_T, R) = \frac{2\rho}{\mu}\sqrt{R^2 \Delta v_T + v_T^2 \Delta R} \tag{18}$$

3.8 Correction factor and calculating some spore charges

From the calculated $d/r = 2.67 \pm 0.28$ value, one can calculate the scaling factor for the geometry by running a FEM simulation for the given ratio. Alternatively, one can compare with figure 16. To find the α-value corresponding to the trap geometry, one measures the distance on the graph from 0 to the tick corresponding to the measured

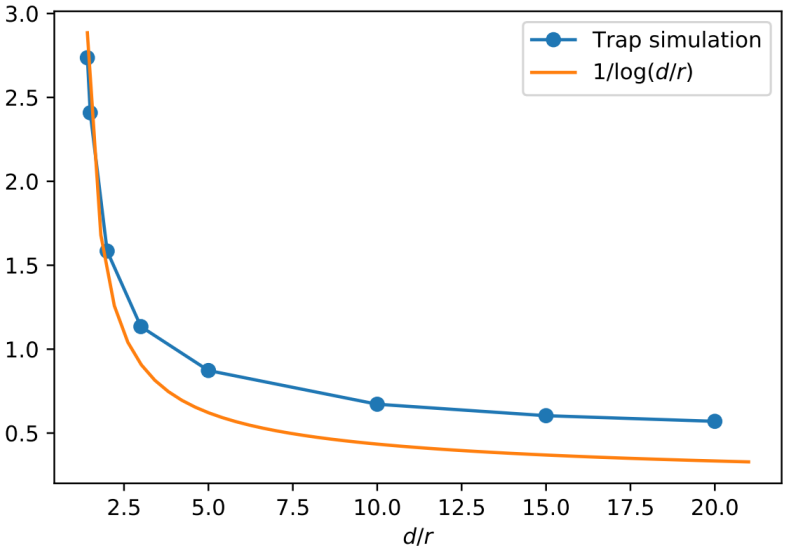

Figure 16: Some simulated α corrections simulated with the FEM method. Additionally plotted one is the correction factor for one electrode as a function of the d/r value [1].

d/r. This is then used as a pixel to mm conversion. One then traces until they hit the blue line, which is a linear interpolation from simulated values – at this point, we draw a straight line to the y-axis, finding the value of α. Performing this leads to $\alpha = 1.40 \pm 0.21$.

The errors are calculated by shifting the initial line with the corresponding errors on the x-axis and finding the α for these points.

We now calculate some sample charges of particles using equations (3) and (5). These values are given in table 5 with a mean of $(444 \pm 80)\,\mathrm{ke}$, with e being the unit charge.

The error propagation for the $E-$field is:

$$\sigma_{E_c} = \frac{1}{d}\sqrt{V_0^2 \Delta\alpha + \alpha^2 \Delta V_0 + \frac{\alpha^2 V_0^2}{d^2}\Delta d} \tag{19}$$

and the error propagation for the charge

$$\sigma_q = \frac{1}{E_c}\sqrt{g^2 \Delta\bar{m} + \alpha^2 \Delta V_0 + \bar{m}^2 \Delta g + \frac{\bar{m}^2 g^2}{E_c^2}\Delta E_c} \tag{20}$$

Particle	Charge in Coulomb [fC]	Charge in thousands of unit charges
1	115.0 ± 21.0	720.0 ± 130.0
2	53.0 ± 9.5	331.0 ± 60.0
3	54.7 ± 9.9	341.0 ± 62.0
4	61.0 ± 11.0	383.0 ± 69.0
5	104.0 ± 19.0	650.0 ± 120.0
6	82.0 ± 15.0	513.0 ± 92.0
7	66.0 ± 12.0	410.0 ± 74.0
8	66.0 ± 12.0	412.0 ± 74.0
9	62.0 ± 11.0	389.0 ± 70.0
10	57.0 ± 10.0	358.0 ± 65.0
11	73.0 ± 13.0	459.0 ± 83.0
12	84.0 ± 15.0	523.0 ± 94.0
13	57.0 ± 10.0	355.0 ± 64.0
14	71.0 ± 13.0	441.0 ± 80.0
15	61.0 ± 11.0	379.0 ± 68.0
Mean	71.0 ± 13.0	444.0 ± 80.0

Table 5: Some calculated charges for the observed particles from 1. In the second column the charge in Couloumb is given and in the third the values are given in terms of thousands of unit charges, $e \approx 1.602\,18 \times 10^{-19}\,\mathrm{C}$.

4 Discussion

4.1 Trap measurements

The expected value for d and r are 4 mm and 2 mm, respectively. That the author estimated $r = 1.5\,0\,13$ means that the real value of r is 4σ from the calculated mean. Most probably, this stems from an underestimation of the error on r.

4.2 Initial observations

The results found by observing the particles in the trap are as expected from section 1 with the oscillation perpendicular to the beam axis from the displacement out of equilibrium due to gravity. However, the more significant non-periodic movements observed along the beam axis were unexpected. This should not be in the case of a singular particle, as the trapping configuration should push the particle back into the middle of the trap by the constant current on the end-caps. A few explanations are possible.

Firstly one reason could be the airflow in the room and especially that two people were working near the trap. Hypothetically, this should not matter due to the windshield, but in practice, the windshield could not be fit perfectly over the trap due to the wiring. This problem was mitigated by meticulously placing the shield while keeping the wiring out of the way. However, this proved insufficient to remove this source of outside influence altogether. After a short time, the wires would be displaced, which displaced the shielding. To solve this in the future, one might affix the wiring to the trap's platform or add a cable guide to minimize the interaction between the wiring and the shielding.

Secondly, it proved impossible to add singular particles with the chosen method of spore charging and trap loading (see section 2). Thus the particles in the trap would experience the electrostatic repulsion from each other. Additionally, the observed particles did not necessarily carry the same charge as some might have gotten more surplus electrons than others. Also, it is unlikely that the observed clusters should consist of singular spores; therefore, in theory, they could carry more charge due to more constituent spores having the same charge. Indeed, the latter process could induce a displacement along the beam axis of the manner observed. Counteracting this displacement involved discharging the Teflon stick and catching surplus clusters, which helped mitigate the described effect but could not solve it entirely as sometimes, when trying to remove the second to last spore, more would fall in. It would be enough to also attract/push the last cluster out of the trapping configuration with either the airflow or direct application of an external electric field. Also, due to the particles being easily airborne when applied to the Teflon, particles were often stuck around the hole in the shielding and also fell upon the bias electrodes, especially those carrying the AC. However, these particles cannot affect the trapping of

the particles, as they would quickly (within 1/50 of a second) assume the electrode's charge. Some did, in any case, wind up getting pushed into the trap by the Teflon stick, getting charged and taking the charge of the instrument, making singular loading more difficult.

When mitigated, this drift should have no significance on the subsequent experiments as they generally do not depend on the particle's position in the trap. However, the particles must not get pushed out of the trap at the end-caps due to excessive airflow (for instance, from movements of the experimenters). This is important in the case of testing the stability of the trapping, as it may end up pushing the particle out of the trapping configuration prematurely.

4.3 Sampling particle at 49, 50, 51 Hz (and continuously)

As mentioned, there was no observable difference between the different sampling rates. This does not correspond to the expected behavior. The predicted behavior derives from the AC oscillation rate, i.e., the oscillation rate of the particles in the trap of 50 Hz. If we sample the oscillation of the particles at the same rate as it oscillates, the particle should seem to be standing still, and when sampling slightly above/below, one expects to see a slow precession of the particle.

That no difference was observed was primarily theorized to stem from the fact that a software-timed method was used to sample the particles' oscillations as the time scale at which the sampling was done was of the order ~ 1 ms. The sampling was implemented in Python via the "time" library, specifically the function "sleep," to wait while the laser was on/off for the duty cycle timing. Python is an interpreted language, and can as such be quite slow, especially function overhead [9] [10] [11]. This means that the de-facto sampling rate/duty cycle was not at the desired 5 ms sampling rate, as the error may have been of the order of the sleep times. A hardware-timed solution, such as hardware PWM, should be implemented for future experiments.

4.4 stability of the trap

The stability of the trap turned out to be better than initially expected, as one could decrease it more than 100 V before the particle started being consequently susceptible to smaller perturbations in the trapping. As mentioned, particular care was taken to have as few particles as possible in the trap when this was investigated.

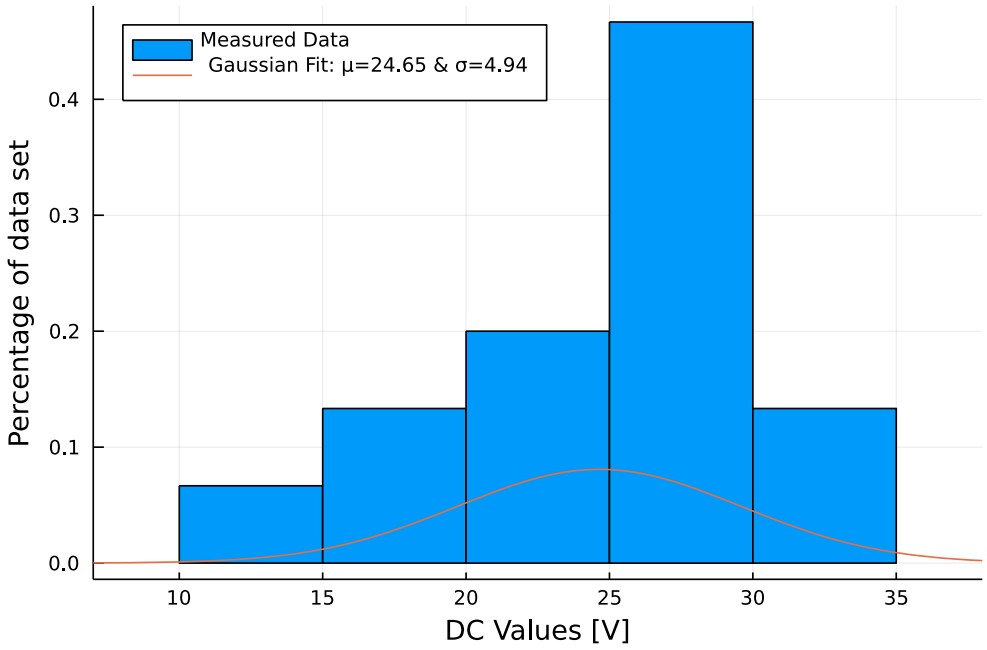

Figure 17: The voltage values from table 5 with a fitted Gaussian. The Gaussian was fitted with the maximum likelihood method, minimizing the maximum likelihood estimator

4.5 Minimizing micromotion

The author expected the DC values minimizing the micromotion to be Gaussian. The assumption was made based on two things. First, the clusters of particles were expected to have a most stable point, with outliers depending on temporary conditions or alternations in the trapping. Thus, it should follow a normal distribution about some mean where the structure is the most stable with deviations depending on small perturbations in the cluster's structure. Assuming a certain amount of charge carried by a particle cluster be proportional to the number of particles in the cluster, one may thus infer that the charge/mass configuration (where the mass should also scale extensively with particle number) should be Gaussian. This assumption has additional support from the central limit theorem, saying sequences of random variables from distributions with well-defined primary moments approach a normal curve [12].

In figure 17 a histogram of the measured voltage values from table 5 are given with a normal distribution fitted to the values. The fit was done using the minimization of a maximum likelihood estimator and served the primary purpose of seeing if the histogram generally followed the expected distribution.

Above in section 2 it was mentioned that the maximum value for the DC source was about 32.5 V, which could again contribute to a bias where some values could not be measured. Though, suppose one fits a normal distribution to the given data and calculates the 95'th percentile. In that case, it comes out to slightly over 32.76 V and the CDF for the value

32.5 V is around 94.4%, reducing the most significant possible effect of this equipment restriction to slightly over 6%. In general, the histogram suggests a normal distribution but has a notable outlier containing more than 40% of the data ranging between 25 V and 30 V.

One reason for this would be that there might be phenomena related to the formation of the particle clusters, which favors configurations that arise at these voltages. However, this is beyond the scope of this study and would have to be done separately.

Another reason could be selection bias. Note how the majority of the data is centered around the range $20\,\mathrm{V} - 30\,\mathrm{V}$, which might be because the charge may scale with the size of the clusters. As particles were partially chosen based on how easily they could be distinguished, this could explain the abnormality in the data, as only a subset of the particle would consistently be sampled. In addition, smaller clusters were often pushed out of the trapping, or otherwise influenced by external parameters, exacerbating the bias.

Finally, considering that the data set has a skewness of about -0.61 and kurtosis of -0.62, one should also consider that there may be another distribution the particles follow or that the detected outliers indeed follow a different distribution or model, which is narrower than that for the rest of the values.

In conclusion: from the author's point of view, the underlying distribution of the particles should follow a Gaussian. Indeed, the data resembled a Gaussian structure during the experiment. However, this model failed to account for a significant outlier, which is interesting as it might mean a stable region where the "outliers" reside. One possible explanation is that the data is governed by two independent mechanisms: the stable part with small perturbations and a greater region where clusters form but have higher variability in their mass and charge. This would be signified by a narrower Gaussian centered where there is now an outlier (25-30 V) and a broader one covering the entirety of the spectrum. Investigating this hypothesis would require an experiment with a more sophisticated way of minimizing the micromotion. Such an experiment would allow for a finer resolution in the detected voltages and sample more clusters, leading to data that could be used to find this out. Again, with this more sophisticated method, particles could be chosen with less bias. Removing human tendency could also elucidate if the outliers in the data are due to this or some underlying reason.

4.6 Measuring radius

The radius was expected to be around $(25 \pm 10)\,\mu\mathrm{m}$, meaning our measurements using the diffraction experiment was about half as big as the expected mean one would ex-

pect. The image analysis of the pixels gave a result much closer to this estimated mean. Additionally, in a previous lab, the author measured the radius of lycopodium spores with diffraction and a microscope, which gave radii of $r_{\text{Diffraction}} = (17.0 \pm 3.5)\,\mu\text{m}$ and $r_{\text{Microscope}} = (16.0 \pm 2.0)\,\mu\text{m}$ respectively [13], lending further credibility to the measurement using the imaging technique.

The author theorizes that the laser measurement's deviation might have originated from measuring the distance between the minima on the Airy disc. As mentioned in section 2 this was done with a ruler, which is much too inaccurate to find the minima consistently. Instead, a picture should have been taken off the airy pattern, seeing as the screen on which it was projected already millimeter incremented, a pixel-m conversion could easily have been found. Improving the accuracy of this measurement technique, edge-detection, thresholding, and filtering could have been used to filter outliers and then find the edges of the airy disc. From this, the center of the dark zones (minima) could have been detected more accurately. That the radius from the diffraction experiment lay within none of the expected intervals could also indicate an underestimate of the errors. The image analysis could also have been improved with the aforementioned tools. Nevertheless, the data matches the expected values quite well.

4.7 Terminal velocity and the Reynolds number

The data found for the terminal velocity value seems reasonable at about 100 mm/s, and mass of $\sim 60\,\text{ng}$ is as such comparable with the estimated mass of $2.5\,\mu\text{g} = 2500\,\text{ng}$. This discrepancy is reasonable given the crudeness of the first mass estimate. The overestimation of the mass by two orders of magnitude most likely stems from assuming r and m would be of the same magnitude, which is false. Assuming the spores are spheres, the expected behavior is $m \sim r^3$ (with the density and other constants left out). A more reasonable guess would, as such, have been around a few ng.

The calculated Reynolds numbers for the different determined radii are also well below 1, mostly on order ~ 0.1 with a mean/standard deviation of $(22.9 \pm 6.2) \times 10^{-2}$, in other words, < 1, assuming that the flow is laminar adequate.

4.8 Spore charges

The average charge was $(71.0 \pm 13.0)\,\text{fC}$, corresponding to $(444.0 \pm 80.0)\,\text{ke}$, with the positive unit charge, which again seems reasonable that on average, the equivalent of 444000 additional electrons would be transferred from the Teflon stick to the clusters. That the value in unit charges is an integer was surprising to the author, as computational errors or other measurement errors were expected to induce errors in the calculations.

The measurements have a relatively high relative error of 19%. To reduce this error, one should, according to equation (20) firstly focus on reducing the error in the mass measurement, as the factor $g^2 \sim 10^2$ dominates the other terms in the error calculation; especially seeing as the error of the voltage is already relatively low.

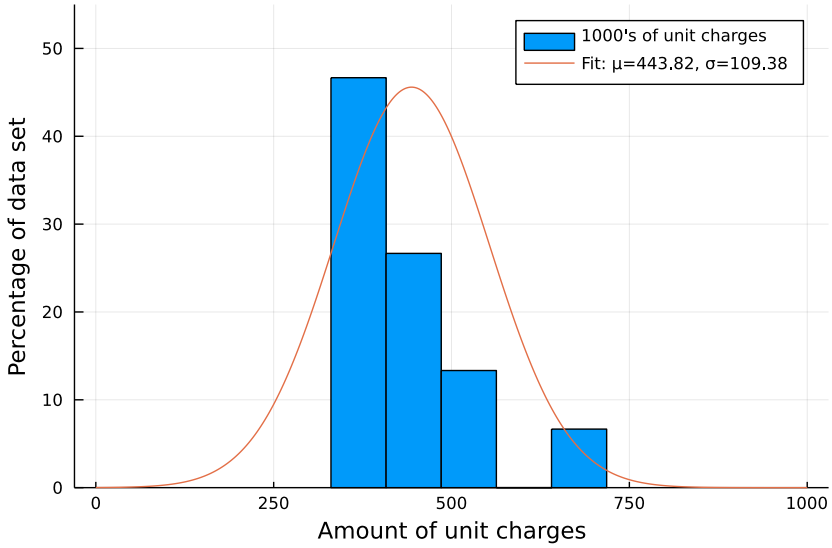

Figure 18: A histogram of the charge data with a fitted normal distribution.

Another crucial point is to consider the normal distribution property of the mass/charge, which should then induce a combination of normal distributions of the charge (products of Gaussian variables are convolutions of their Gaussians). Unfortunately, as seen in figure 18, this is again not an accurate statement but could be with a larger data set.

The bias may be negated by implementing a way to find the particles, improve the granularity of the DC voltage and take more data. Finally, one should consider if a different distribution may fit better to the charge distribution on the spore clusters.

5 Conclusion

In this study, a quadrupole ion trap combined with elementary experimental techniques was used to determine the average mass, radius, and acquired charge of lycopodium spores. For future research, these values could be measured more precisely by applying more advanced image processing techniques, improving the range and precision of the DC voltages, and investigating the underlying distribution of the masses and charges.

A Safety considerations

A.1 Working with electricity

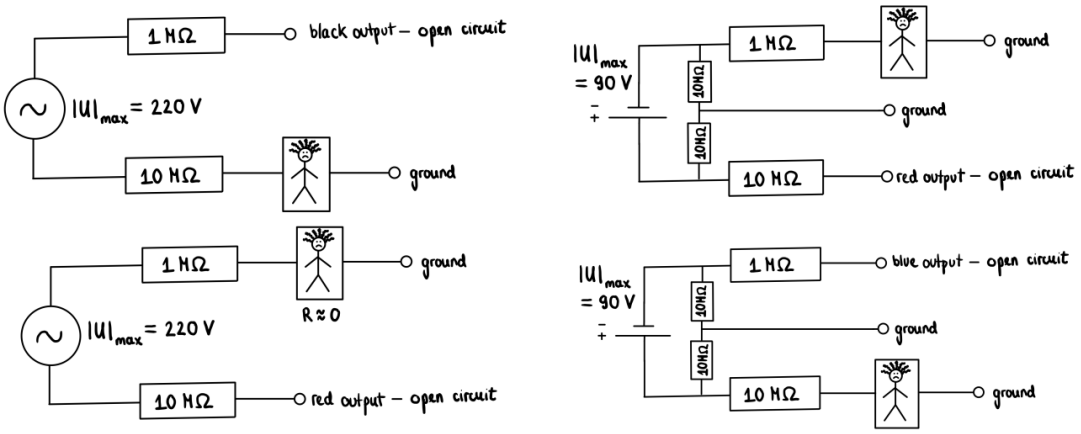

Figure 19: The possible scenarios in which an experimenter could come into contact with live current in this experiment. The scenarios are marked numerically as: 1 (top left), 2 (bottom left), 3 (top right), 4 (bottom right)

Using the situations given in 19 and assuming $R_{\text{Human}} = 0$, and that no current flows in the open circuit direction, we can acquire upper bounds for the maximum current which may flow through an experimenters body. In the following equations, the I indices refer to figure 19 and the numbering described in the caption.

$$I_1 = \frac{220\,\text{V}}{10\,\text{M}\Omega} = 22\,\mu\text{A} \qquad I_3 = \frac{90\,\text{V}}{10\,\text{M}\Omega} = 0.09\,\text{mA}$$
$$I_2 = \frac{220\,\text{V}}{1\,\text{M}\Omega} = 22\,\mu\text{A} \qquad I_4 = \frac{90\,\text{V}}{10\,\text{M}\Omega} = 9\,\mu\text{A}$$

Assuming the safe current is 1 mA, one can clearly see that in all scenarios we are well below the safe current.

When working with electrical equipment, one should also pay special attention to the safe limits for the equipment. This may be mitigated by adding additional resistors, as the operating voltage/current are mostly far below the safe values.

A.2 Lasers

The laser used in the experiment has enough power to be classed as a class 3 laser though, it is not focused. This means that the effective W/m^2 is low.

In any case, no jewelry nor watches should be carried to avoid reflections of the laser light and also avoid looking into the laser.

B Code for the Raspberry Pi

B.1 Constant beam

In this listing, a program to continuously deliver a signal to a pin is displayed.

```
import wiringpi

wiringpi.wiringPiSetupGpio() # setup GPIO numbering
wiringpi.pinMode(18 , 1)     # declare 18 as an output pin

wiringpi.digitalWrite(18, 1) # write signal "on" to the pin

input("")                    # wait until enter is pressed
wiringpi.digitalWrite(18, 0) # write signal "off" to the pin
```

B.2 Software modulation

In the following listing, an example of how one can create a software-based solution for flashing the laser at a certain frequency.

```
import wiringpi

T = 1 # total time of one cycle
d = 0.5 # duty cycle: how many % of the time is the laser on?

while True:
    wiringpi.wiringPiSetupGpio()    # setup GPIO
    wiringpi.softToneCreate(17)     # create oscillation on 17

    wiringpi.softToneWrite(17, 50) # start oscillation at 50Hz
    time.sleep(d * T)              # sleep: keep laser on

    wiringpi.digitalWrite(17, 0)   # turn off the laser
    time.sleep((1-d) * T)   # laser off for remainder of cycle
```

For instance if one wants to have the laser on for 5ms, then one should choose $T = 1$ and $d = 0.005$ (0.5 %).

B.3 Pulse-width modulation

```
import RPi.GPIO as Io

Io.setmode(Io.BCM)  # we are using BCM ordering
Io.setup(19,Io.OUT)  # initialize GPIO19 as an output.

p = Io.PWM(19, 100)  # GPIO19 as PWM output, 100Hz frequency
p.start(50)          # create PWM signal with 50% duty cycle
input("")            # wait until enter is pressed
p.ChangeDutyCycle(0) # turn of the modulation
GPIO.cleanup()       # clean up the traces of the program
```

For further documentation, see [14] and [15].

C Data sheet for the laser

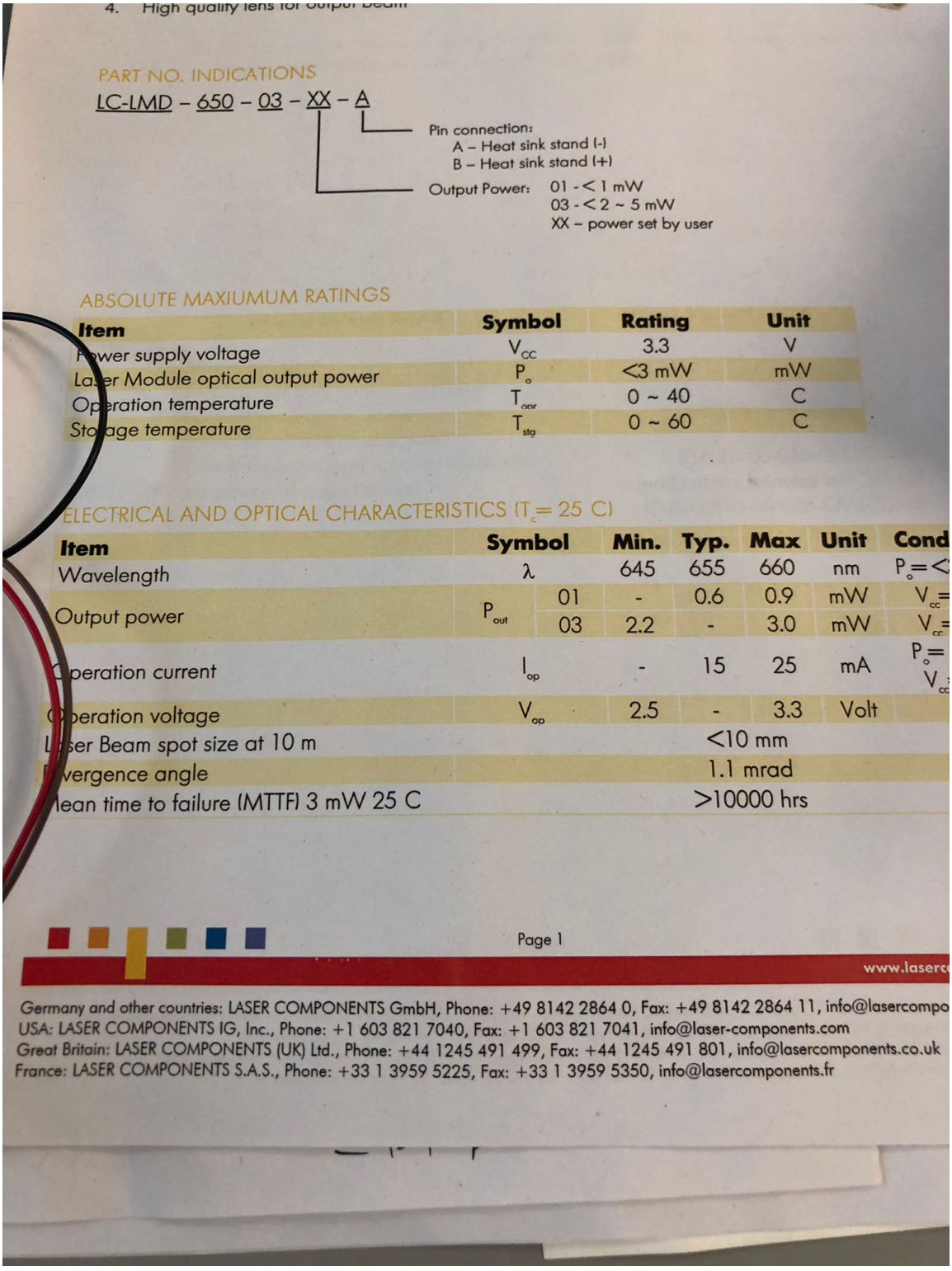

4. High quality lens for output beam

PART NO. INDICATIONS

LC-LMD – 650 – 03 – XX – A

Pin connection:
A – Heat sink stand (-)
B – Heat sink stand (+)

Output Power: 01 - < 1 mW
03 - < 2 ~ 5 mW
XX – power set by user

ABSOLUTE MAXIUMUM RATINGS

Item	Symbol	Rating	Unit
Power supply voltage	V_{CC}	3.3	V
Laser Module optical output power	P_o	<3 mW	mW
Operation temperature	T_{opr}	0 ~ 40	C
Storage temperature	T_{stg}	0 ~ 60	C

ELECTRICAL AND OPTICAL CHARACTERISTICS (T_c= 25 C)

Item	Symbol		Min.	Typ.	Max	Unit	Cond
Wavelength	λ		645	655	660	nm	P_o=<
Output power	P_{out}	01	-	0.6	0.9	mW	V_{cc}=
		03	2.2	-	3.0	mW	V_{cc}=
Operation current	I_{op}		-	15	25	mA	P_o= V_{cc}
Operation voltage	V_{op}		2.5	-	3.3	Volt	
Laser Beam spot size at 10 m				<10 mm			
Divergence angle				1.1 mrad			
Mean time to failure (MTTF) 3 mW 25 C				>10000 hrs			

Page 1

www.laserc

Germany and other countries: LASER COMPONENTS GmbH, Phone: +49 8142 2864 0, Fax: +49 8142 2864 11, info@lasercompo
USA: LASER COMPONENTS IG, Inc., Phone: +1 603 821 7040, Fax: +1 603 821 7041, info@laser-components.com
Great Britain: LASER COMPONENTS (UK) Ltd., Phone: +44 1245 491 499, Fax: +44 1245 491 801, info@lasercomponents.co.uk
France: LASER COMPONENTS S.A.S., Phone: +33 1 3959 5225, Fax: +33 1 3959 5350, info@lasercomponents.fr

Figure 20: Data sheet of the laser used for the experiment.

References

[1] D-PHYS: Mordini Carmelo. Quadrupole ion trap. *ETH AP Experiments*, 2021.

[2] Wolfgang Paul. Electromagnetic traps for charged and neutral particles. *Rev. Mod. Phys.*, 62:531–540, Jul 1990.

[3] John D. Jackson. *Classical Electrodynamics*. Wiley, New York, 1998.

[4] Hugh D. Young and Roger A. Freedman. *University Physics with Modern Physics*. Pearson, Essex, 2016.

[5] Jing Wang. Lecture script air pollution control ii, environmental engineering. Available upon request.

[6] Raspberry Pi Foundation. Raspberry pi os. Report, Raspberry Pi, 2021.

[7] Apple Inc. iphone x - technical specifications. Report, RAND Corporation, 2021.

[8] Eidgenössisches Institut für Meterologie METAS. Die gravitationszonen der schweiz. `https://www.metas.ch/metas/de/home/dok/gravitationszonen.html`. Accessed: 07.11.2021.

[9] Micha Gorelick and Ian Ozsvald. *High Performance Python: Practical Performant Programming for Humans*. O'Reyilly, Sebastopol, 2020.

[10] Mohamed Ismail and G. Edward Suh. Quantitative overhead analysis for python. In *2018 IEEE International Symposium on Workload Characterization (IISWC)*, pages 36–47, 2018.

[11] Guido van Rossum. Google + post. `https://web.archive.org/web/20180919031245/https://plus.google.com/115212051037621986145/posts/HajXHPGN752`. Accessed: 11.11.2021.

[12] Louis Lyons. *Statistics for nuclear and particle physicists*. Cambridge University Press, The Edinburgh Building, Cambridge, 1986.

[13] Marcus Mähring and Johannes Eberle. 16, light interference and diffraction effects. From the Praktikum I course, available upon request.

[14] Ben Croston. Rpi.gpio 0.7.0. Documentation, Independent, 2020.

[15] Gordon Henderson. Wiring pi, gpio interface library for the raspberry pi. Documentation, Wiring Pi Project, 2021.